PSFC/JA-10-64

Continuous-Wave Operation of a Frequency Tunable 460 GHz Second-Harmonic Gyrotron for Enhanced Nuclear Magnetic Resonance

Torrezan, A.C., Han, S.T., Mastovsky, I., Shapiro, M.A., Sirigiri, J.R., Temkin, R.J., Barnes, A.B.*, Griffin, R.G.*

* Department of Chemistry and the Francis Bitter Magnet Laboratory, Massachusetts Institute of Technology, Cambridge, MA 02139

2010

Plasma Science and Fusion Center
Massachusetts Institute of Technology
Cambridge MA 02139 USA

This work was supported by the U.S. National Institutes of Health under Grant EB004866.

Continuous-Wave Operation of a Frequency Tunable 460 GHz Second-Harmonic Gyrotron for Enhanced Nuclear Magnetic Resonance

Antonio C. Torrezan, *Student Member, IEEE*, Seong-Tae Han†, Ivan Mastovsky, Michael A. Shapiro, *Member, IEEE,* Jagadishwar R. Sirigiri, *Member, IEEE*, Richard J. Temkin, *Fellow, IEEE,* Alexander B. Barnes, and Robert G. Griffin

***Abstract*—The design, operation and characterization of a continuous-wave (CW) tunable second-harmonic 460 GHz gyrotron are reported. The gyrotron is intended to be used as a submillimeter-wave source for 700 MHz nuclear magnetic resonance (NMR) experiments with sensitivity enhanced by dynamic nuclear polarization (DNP). The gyrotron operates in the whispering gallery mode $TE_{11,2}$ and has generated 16 W of output power with a 13-kV 100-mA electron beam. The start oscillation current measured over a range of magnetic field values is in good agreement with theoretical start currents obtained from linear theory for successive high order axial modes $TE_{11,2,q}$. The minimum start current is 27 mA. Power and frequency tuning measurements as a function of the electron cyclotron frequency have also been carried out. A smooth frequency tuning range of 1 GHz was obtained for the operating second-harmonic mode either by magnetic field tuning or beam voltage tuning. Long-term CW operation was evaluated during an uninterrupted period of 2 days, where the gyrotron output power and frequency were kept stable to within ±0.7% and ±6 ppm, respectively, by a computerized control system. Proper operation of an internal quasi-optical mode converter implemented to transform the operating whispering gallery mode to a Gaussian-like beam was also verified. Based on images of the gyrotron output beam taken with a pyroelectric camera, the Gaussian-like mode content of the output beam was computed to be 92% with an ellipticity of 12%.**

***Index Terms*—Dynamic nuclear polarization (DNP), nuclear magnetic resonance (NMR), second cyclotron harmonic, submillimeter wave, terahertz, tunable gyrotron.**

I. Introduction

One of the scientific applications that have been driving the development of medium-average power electromagnetic sources in the millimeter and submillimeter-wave bands is sensitivity-enhanced nuclear magnetic resonance (NMR) via dynamic nuclear polarization (DNP). In DNP/NMR, signal enhancement up to two orders of magnitude [1]-[3] can be obtained by transferring the high polarization of electron spins to nuclear spins through irradiation of a sample under study with electromagnetic waves at a frequency close to the electron Larmor frequency. In order to combine this signal enhancement technique with the improved spectral resolution and sensitivity provided by contemporary NMR spectrometers operating at magnetic fields greater than 5 T, microwave sources operating at frequencies higher than 140 GHz and able to deliver several watts to several tens of watts of output power are needed [1]. Long-pulse or continuous-wave (CW) operation with highly stable output power and frequency are also required from these sources in order to enable a complete transfer of polarization [2] and long-term signal averaging in DNP experiments [3]. Another desirable feature that would simplify DNP operation is smooth frequency tunability where maximum signal enhancement could be obtained by tuning the microwave frequency instead of changing the NMR magnetic field. In addition, tunable sources would permit the implementation

of DNP in current NMR spectrometers without the need for a sweep coil.

Among submillimeter sources available to date, solid-state sources such as IMPATT and Gunn diodes have power capability limited to hundreds of mW and tens of mW at 140 GHz, respectively, dropping to a few mW at 300 GHz [4]. A solid state DNP source consisting of an oscillator connected to an amplifier and a chain of frequency multipliers is able to deliver a maximum output power of 33 mW at 264 GHz with a 3-dB frequency tuning range of 13.9 GHz [5]. Optically pumped far-infrared (FIR) lasers can provide a series of discrete lines between 0.16 and 7.5 THz [6], with maximum power of 1.2 W at 2.5 THz [7] reducing to a few mW below 600 GHz in commercial versions [8], [9]. In the realm of vacuum electron devices, conventional tubes based on Cherenkov radiation utilize slow-wave structures with transverse dimensions on the order of the wavelength in order to provide waves with subluminal phase velocity to interact with an electron beam. At high frequencies, these structures become more involved to fabricate and have limited average power capability. For example, even though commercially available extended-interaction oscillators (EIO) are able to generate 25 W of power at 140 GHz at continuous duty, the output power of these devices reduces to 1 W at 220 GHz [10]. Backward-wave oscillators (BWO), which have covered frequencies up to 1.4 THz, follow a similar trend with power dropping from about 10 W at 140 GHz to 1 W at 300 GHz [11].

On the other hand, fast-wave vacuum electron devices such as gyrotrons allow interaction between electrons and waves with superluminal phase velocity. These fast waves are supported by overmoded smooth waveguides, which are simpler to fabricate and able to handle the average power required for DNP/NMR and beyond. For instance, a gyrotron oscillator developed for fusion application has produced MW power levels at 170 GHz for a pulse length as long as 800 s [12]. Gyrotrons operating at the second harmonic of the cyclotron frequency have generated kW power levels in the CW regime at 157, 250, and 326 GHz [13], [14].

Gyrotrons were first developed for high-field DNP/NMR at the Massachusetts Institute of Technology (MIT, Cambridge, USA) in the early 1990s initially at 140 GHz [15] and later at 250 GHz [16], corresponding to 211 and 380 MHz ^{1}H NMR frequencies, respectively. These gyrotrons operate at the fundamental harmonic of the cyclotron frequency and have generated 14 W at 140 GHz [17] and 7 W at 250 GHz [3] using low beam power (300 W) and low beam current (25 mA). Long-term continuous operation with stable output power and frequency has been demonstrated for both gyrotrons. In particular, the 250 GHz gyrotron has achieved uninterrupted and stable CW operation for a period of 21 days [3]. The possibilities and results [1]-[3], [15] provided by this new instrumentation have sparked the interest of other research laboratories [18]-[20] and companies [21] around the world which are employing or developing gyrotrons for DNP/NMR spectrometers.

In order to extend the applicability of DNP/NMR to higher fields, the expensive cost of 10-22 T Nb_3Sn superconducting magnets can be avoided by operating the gyrotron at a cyclotron harmonic while utilizing less expensive NbTi superconducting magnets with fields up to 10 T. This option was first considered at MIT with the development of a second-harmonic 460 GHz gyrotron for a 700 MHz ^{1}H NMR system [22]. The first version of this gyrotron was able to generate up to 8.4 W of output power for a 12.4-kV 135-mA electron beam. The start current of the operating mode $TE_{0,6}$ was measured to be 67 mA and stable continuous operation was demonstrated for a period of 1 hour [23]. Another second-harmonic gyrotron was developed later at University of Fukui, Fukui, Japan, for a 600 MHz DNP/NMR system [18]. Prospects to employ DNP to even higher NMR frequencies may be envisaged from a recent demonstration of 1 THz generation from a CW second-harmonic gyrotron [24].

A useful feature observed in the MIT 250 GHz and 460 GHz gyrotrons was continuous frequency tunability due to the excitation of successive high order axial modes as a function of magnetic field [2], [22]. While a tuning range broader than 2 GHz was observed for fundamental modes, the continuous frequency tunability of second-harmonic modes was limited to a mere 50 MHz. Wideband magnetic tuning, similar to the tuning reported in [22], has recently been reported in a 140 GHz gyrotron oscillator, with up to 6 GHz of magnetic tuning obtained [25]. For low frequencies gyro-devices operating at the second cyclotron harmonic, smooth broadband magnetic tuning of 2.2 GHz has been observed in a 25-GHz CW gyro-BWO [26].

In this paper, we report the operational characteristics of a second-harmonic 460 GHz CW gyrotron. The tube was redesigned and rebuilt from a previous version for higher output power, lower start

current, and improved stability/reliability. Broadband smooth frequency tunability by changing the electron cyclotron frequency was also obtained for the operating second-harmonic mode. This paper is organized as follows: Section I describes the design and features of the different parts of the tube, including electron gun, cavity interaction region, and internal converter from a cylindrical waveguide mode to a linearly polarized free space Gaussian-like beam. Evaluation of output power and frequency tunability as a function of magnetic field and beam voltage, start oscillation current of the operating mode, ohmic loss, frequency and power stability in long-run continuous operation, and output microwave beam profile are detailed in Section III. The paper is finalized with conclusions in Section IV.

II. Design

A schematic of the upgraded 460 GHz second-harmonic gyrotron is shown in Fig. 1, which depicts the different parts of the tube: electron gun, cavity interaction region, internal mode converter, and collector.

A. Diode Electron Gun

The magnetron injection gun utilized in this work kept the same diode configuration and geometry of the previous version of the tube [22]. After being thermionically emitted from an indirectly heated ring cathode of radius 5.38 mm and slant length 1.09 mm, electrons are accelerated due to a potential difference between a grounded anode and a cathode at a beam voltage $-V_b$. As the electrons advance through the beam tunnel in cyclotron motion around the magnetic field lines created by the main superconducting magnet, the hollow annular electron

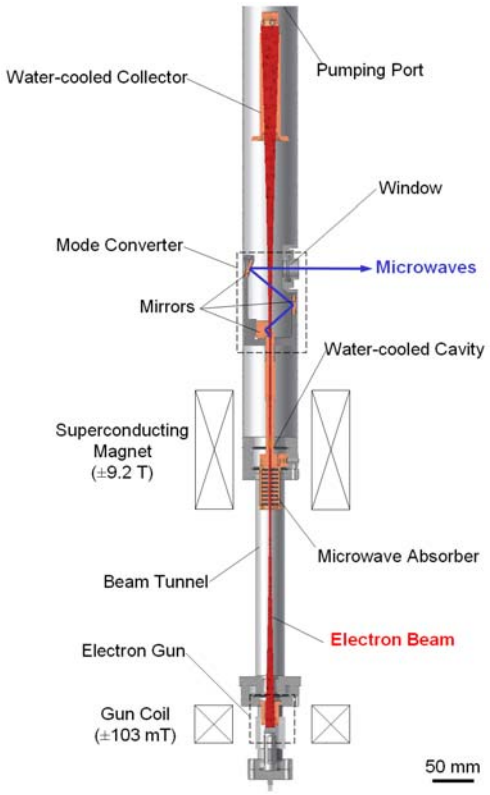

Fig. 1. 460 GHz gyrotron schematic.

beam is compressed, reaching a final beam radius of r_b = 1.1 mm in the cavity interaction region. The electron gun geometry is depicted in Fig. 2(a) along with equipotential lines, and electron trajectories obtained from the code EGUN [27] for the gyrotron operating parameters V_b = 13 kV and beam current I_b = 100 mA. Other important beam parameters, namely the ratio of perpendicular to axial electron velocity known as pitch factor α and the beam perpendicular velocity spread $\Delta v_\perp/v_\perp$, were also evaluated at the

cavity region using EGUN. The results from these simulations are shown in Fig. 2(b) and a set of values favorable for beam-wave interaction, i.e. a high pitch factor ($\alpha \cong 2$) and a low perpendicular velocity spread (($\Delta v_\perp / v_\perp$) < 4%), was obtained at the operating voltage V_b = 13 kV by proper adjustment of a water-cooled copper gun coil with a magnetic field range of ±103 mT.

B. Interaction Circuit

Although operation at the second-harmonic of the cyclotron frequency has the advantage of requiring only half of the magnetic field demanded for a fundamental harmonic mode, second-harmonic modes suffer from lower beam-wave interaction efficiency and from additional competition with neighboring fundamental modes. In order to overcome these difficulties, the $TE_{11,2}$ mode was chosen as the operating mode due to its isolation from surrounding modes and its high coupling to an electron beam of radius 1.1 mm. This whispering-gallery mode is supported by a 30-mm long

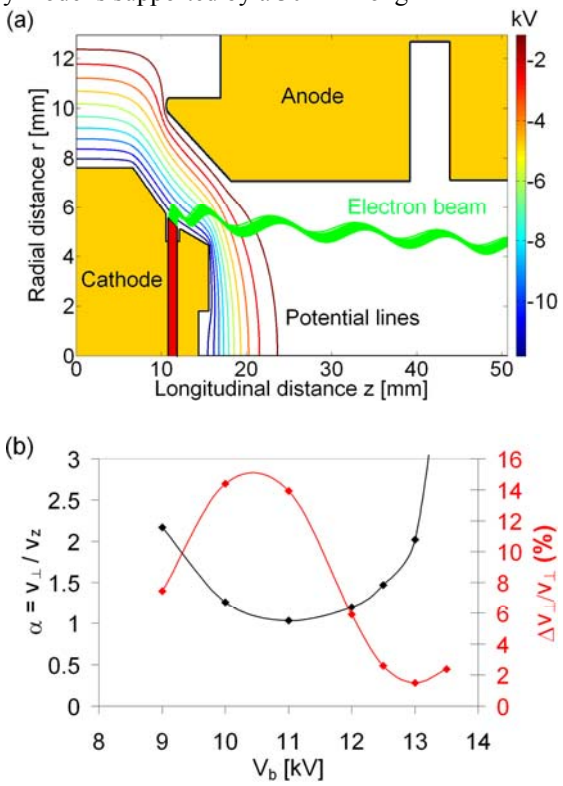

Fig. 2. (a) Magnetron injection gun geometry, and simulated electron trajectories and equipotential lines for an applied voltage V_b = 13 kV and beam current I_b = 100 mA; (b) Computed pitch factor α and beam perpendicular velocity spread $\Delta v_\perp / v_\perp$ at the cavity entrance according to the code EGUN. The gun coil field was adjusted to a subtracting field of –61 mT for high α and low spread at the operating voltage 13 kV.

cylindrical cavity with radius r_{cav} = 1.825 mm, where a long cavity (~ 46 λ at 460 GHz, where λ is the free-space wavelength) was preferred in order to reduce the start oscillation current. The interaction circuit geometry comprising a cavity straight section and tapered sections is shown in Fig. 3. Also shown in Fig. 3 is the axial electric field profile of the first axial mode $TE_{11,2,1}$ calculated from a cold-cavity code [28].

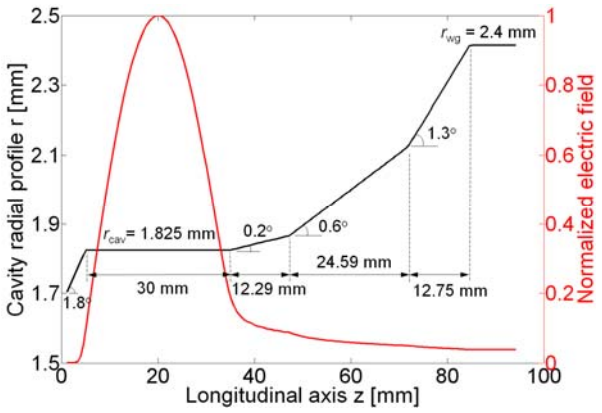

Fig. 3. Schematic of the 460 GHz gyrotron circuit featuring a downtaper section, cavity (straight section), and uptaper section. The red line represents the normalized axial electric field profile of the operating mode $TE_{11,2,1}$.

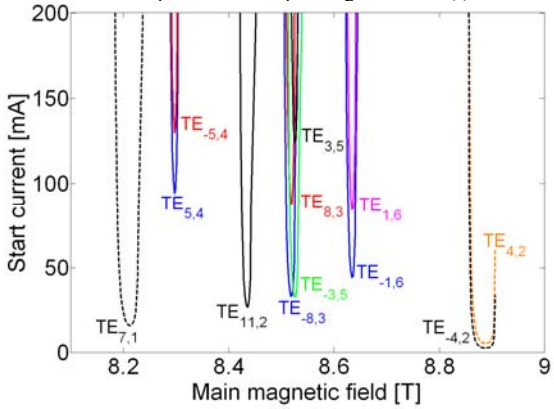

Fig. 4. Start oscillation current of cavity $TE_{m,n,1}$ modes in the vicinity of the operating mode $TE_{11,2,1}$. Dashed lines represent fundamental harmonic modes while solid ones refer to second-harmonic modes (Beam parameters: V_b = 12.8 kV, r_b = 1.1 mm, α = 1.85, no velocity spread).

The gyrotron cavity was manufactured by electroforming where oxygen-free copper was deposited on an aluminum mandrel precisely machined to a tolerance of 2.5 μm in cavity diameter. After fabrication, the gyrotron cavity was cold tested and the cavity radius was estimated to be 1.823 mm, corresponding to a cutoff frequency of 460.65 GHz for the $TE_{11,2,1}$ mode. The cold test consisted of exciting lower order cavity modes such as TE_{01} and TE_{12} by means of a step-cut Vlasov converter and measuring the respective resonant frequencies using a vector network analyzer Agilent E8363B with a 90-140 GHz extension. Once the measured frequencies were corrected for a vacuum environment [29], the cold cavity code was utilized to determine the cavity radius that would match the corrected frequency.

Based on linear theory [30] and the cold axial electric field profile, the start current of the $TE_{11,2,1}$ mode was computed to be 27 mA for beam parameters V_b = 12.8 kV, α = 1.85, and no velocity spread. Following similar procedure, the start current of the surrounding modes was also evaluated and the result is shown in Fig. 4, which demonstrates the isolation of the operating second harmonic mode from surrounding modes, especially fundamental modes. The nomenclature $TE_{m,p,q}$ denotes a cylindrical TE cavity mode with a radial mode number p, axial mode number q, and azimuthal mode number m, where a positive m refers to a mode co-rotating with respect to the electron gyration while a negative m refers to a counter-rotating mode.

C. Internal Mode Converter and Collector

After transferring part of their perpendicular energy to the generated wave, the spent beam is separated from the electromagnetic wave by an internal mode converter and it is allowed to expand in the decaying field of the superconducting magnet until is collected on a water-cooled copper collector at ground potential. Meanwhile, a portion of the generated wave diffracts out of the resonator and propagates

through the uptaper section followed by an output cylindrical waveguide of radius r_{wg} = 2.4 mm.

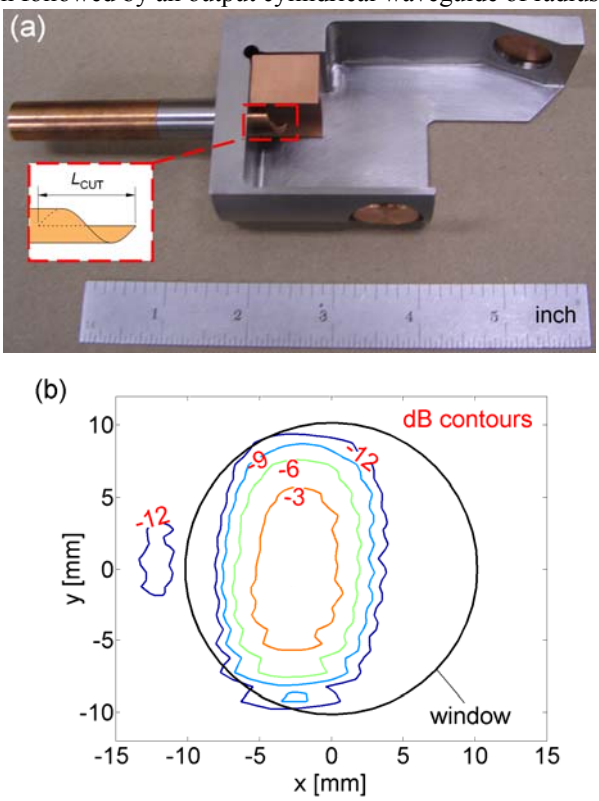

Fig. 5. (a) Quasi-optical mode converter picture with inset showing the helical launcher orientation, (b) simulated electric field profile of the mode-converted $TE_{11,2}$ output beam at the window plane at 460 GHz.

Mode conversion in the uptaper part was found to be less than 0.2% according to calculations using the scattering matrix code Cascade [31]. In the sequence, the cylindrical mode is internally converted to a linearly polarized free-space Gaussian-like beam, which is suitable for low-loss transmission to the NMR probe using a corrugated waveguide.

The internal mode converter is depicted in Fig. 5a and consists of a helical launcher, a quasi-parabolic mirror, and two flat mirrors to deflect the microwave beam out of the tube through a transparent fused silica window of diameter 20.3 mm and thickness 2.00 mm, and a horizontal cross bore in the superconducting magnet. The converter design is based on a geometrical optics approach [32], where the helical cut length was determined by:

$$L_{CUT} = 2\cot\theta_B r_{wg}\sqrt{1-\left(\frac{r_c}{r_{wg}}\right)^2}\,\frac{\pi}{\theta} \qquad (1)$$

where $\theta_B = \arcsin(k_\rho/k)$ is the Brillouin angle, $r_c = r_{wg}(m/\nu'_{mp})$ is the caustic radius, and $\theta = \arccos(r_c/r_{wg})$ is the azimuthal bounce angle. Here k denotes the free space wavenumber and $k_\rho = \nu'_{mp}/r_{wg}$ denotes the transverse wavenumber of the TE_{mpq} mode, where ν'_{mp} is the p^{th} nonvanishing zero of the derivative of the Bessel function $J_m'(x)$. For the $TE_{11,2}$ mode and output waveguide r_{wg} = 2.4 mm, one has L_{CUT} = 11.2 mm, $\theta_B = 49.5^o$, $r_c/r_{wg} = 0.625$, and $\theta = 51.3^o$.

The design was evaluated using an electric field integral equation code Surf3D [33] and the computed electric field profile of the mode-converted $TE_{11,2}$ output beam at 460 GHz is shown in Fig. 5b. The simulated field profile has a Gaussian-like content of 92% with beam radii w_x = 5.6 mm and w_y = 8.7 mm at the window plane.

III. Experimental Results

The new version of the 460 GHz second-harmonic gyrotron was entirely processed and characterized in CW mode, with total beam transmission from the electron gun to the collector. The use of a relatively low electron beam power (< 15 kV, < 150 mA) and adequate water cooling in sensitive parts of the device such as anode, cavity, collector, and gun coil, contributed to achieving complete CW operation. Another factor that assists in this task is the internal mode converter configuration, which not only allows a reduction of the thermal load on the collector but also permits a better vacuum pumping conductance throughout the tube. For example, electron beam power in excess of 1.5 kW has been dissipated on the collector without noticeable side effects. The temperature in the cooling channels was kept stable by a 2.4 kW recirculating chiller, with the water temperature and flow at each channel being monitored by flowmeters. Relays existent in these flowmeters and in the ion pump controller formed a hardware safety interlock network ready to shut off the beam voltage if necessary. Software interlocks were also implemented in the computer control routine.

The output power was monitored at the end of a corrugated waveguide connected to the gyrotron window using, unless otherwise specified, a Scientech laser calorimeter model SN4177 calibrated for the submillimeter wavelength range. The corrugated waveguide employed in these measurements has an inner diameter of 19 mm and a corrugation depth of $\lambda/4$ [34]. The gyrotron frequency was measured using a heterodyne system, which consists of a harmonic mixer, an 18-26 GHz YIG-tuned local oscillator, a Phase Matrix 578B frequency counter utilized to monitor the local oscillator frequency, and an intermediate frequency section. The main gyrotron operating parameters are summarized in Table I.

A. Start Oscillation Current

The start oscillation current of the operating mode $TE_{11,2}$ was measured as a function of magnetic field for a fixed beam

TABLE I
GYROTRON OPERATING PARAMETERS

Operating mode $TE_{m,p,q}$	$TE_{11,2,q}$
Frequency	460.2 GHz
Magnetic/voltage tuning range	1.0 GHz
Cavity magnetic field B_0	8.42 T
Cyclotron harmonic	Second
Beam voltage V_b	13 kV
Beam current I_b	100 mA
Output power	16 W (CW)

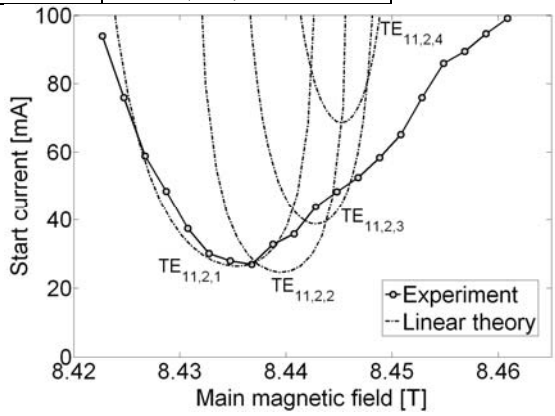

Fig. 6. Measured start oscillation current (solid line) of the operating mode $TE_{11,2}$ as a function of magnetic field for beam voltage V_b = 12.8 kV and gun coil field of –75 mT. Theoretical start currents based on linear theory for the first four axial modes $TE_{11,2,q}$, where q = 1, 2, 3, 4, are represented by dash-dotted lines (Simulation parameters: r_{cav} = 1.822 mm, cold axial electric field profile, and beam parameters V_b = 12.8 kV, α = 1.85, with no velocity spread).

voltage V_b = 12.8 kV and gun coil field of –75 mT. The result from this measurement is shown as a solid line in Fig. 6 and it is compared to theoretical start currents obtained from linear theory for the first four axial modes $TE_{11,2,q}$, where q = 1, 2, 3, 4. In these calculations, the axial electric field profile obtained from a cold cavity code was employed and the following beam parameters were assumed, V_b = 12.8 kV, α = 1.85, and no velocity spread. The cavity radius was chosen to be r_{cav} = 1.822 mm for best fit, which is within experimental error of the value (1.823 mm) obtained from the cavity cold test.

Good agreement between the measured and theoretical start current for the first axial mode $TE_{11,2,1}$ is obtained at lower magnetic field values (< 8.44 T), where the minimum start current was measured to be 27 mA. This represents a start current much lower than the 67 mA measured for the operating mode $TE_{0,6}$ in the previous version of the 460 GHz gyrotron [22]. The wider range of excitation of the measured start current compared to the magnetic field range of the theoretical start current for the $TE_{11,2,1}$ mode suggests that high order axial modes ($q \geq 2$) are being observed in the experiment, which is in reasonable agreement with the calculated start currents for high order axial modes $TE_{11,2,q}$, q = 2, 3, 4.

B. Power and Frequency Tuning

The 460 GHz gyrotron has generated 16 W of output power in the $TE_{11,2,1}$ second-harmonic mode for a 13-kV 100-mA electron beam, yielding an efficiency of 1.2%, a significant improvement compared to the previous configuration of this tube [23]. In addition, a smooth frequency tuning range of 1 GHz has been measured as a function of magnetic field for a constant 13-kV 100-mA electron beam as shown in Fig. 7. This represents a tuning range twenty times broader than previously reported for a second-harmonic mode in a high- frequency gyrotron. In the magnetic tuning measurement, the gyrotron output power was optimized by adjusting the subtracting gun coil field from –75 mT to –78 mT as the main magnetic field was increased, resulting in a minimum output power of 2 W throughout the tuning band.

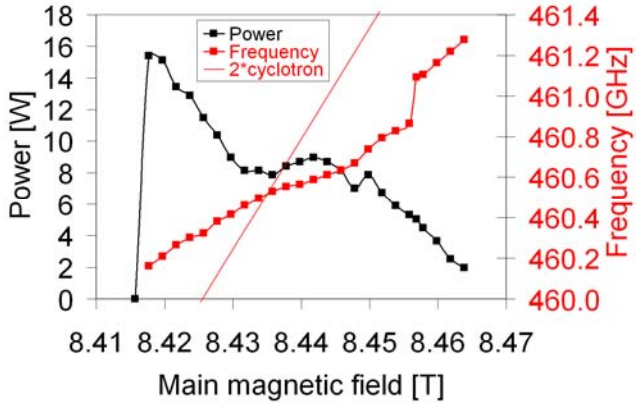

Fig. 7. Power and frequency tuning measurement as a function of magnetic field for the $TE_{11,2}$ mode, beam current I_b = 100 mA, and beam voltage V_b = 13 kV. The gun coil was swept from –75 mT to –78 mT for best output power as the magnetic field was increased.

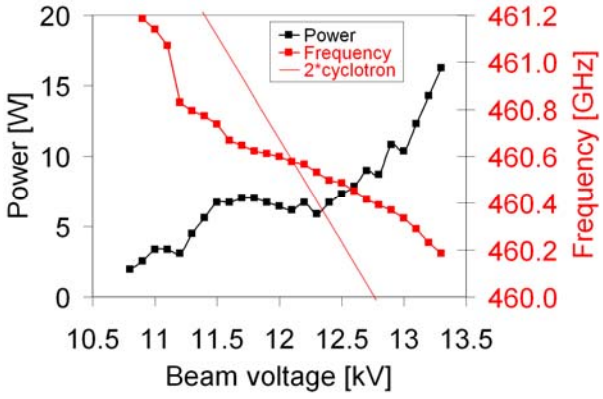

Fig. 8. Power and frequency tuning measurement as a function of beam voltage for the $TE_{11,2}$ mode, beam current I_b = 100 mA, and main magnetic field B = 8.422 T. The gun coil was swept from –71 mT to –103 mT for best output power as the beam voltage was decreased from the maximum power point.

Tuning measurements were also performed by changing the beam voltage while keeping the main magnetic field at B = 8.422 T and the beam current at I_b = 100 mA. The voltage tuning results are presented in Fig. 8, with similar output power and frequency tuning range compared to the magnetic tuning case. As the beam voltage was decreased from the maximum output power value, the gun coil had to be swept from –71 mT to –103 mT in order to keep a high α in the diode gun configuration for best output power.

As suggested by the start current measurement, the excitation of successive high order axial modes $TE_{11,2,q}$ plays a role in providing the extended tuning as one increases the magnetic field for a fixed beam voltage or decreases the beam voltage for a constant main magnetic field. Electron beam interaction with backward-wave components of high order axial modes is also observed and it occurs in a region where the gyrotron radiation frequency is less than the second harmonic of the electron cyclotron frequency. For the magnetic tuning case in Fig. 7, the backward interaction region corresponds to magnetic field values greater than $B \cong 8.44$ T, a transition region from the mode $TE_{11,2,1}$ to $TE_{11,2,2}$ as suggested by the start current measurement in Fig. 6. For the voltage tuning case in Fig. 8, the backward interaction region corresponds to $V_b < 12.1$ kV.

C. Ohmic Loss

At high frequency operation, a significant part of the power transferred from the electron beam is not extracted from the gyrotron cavity but instead it is deposited in the cavity walls as ohmic loss. By measuring the water flow rate in the cavity cooling channel and the difference between its inlet and outlet temperature using thermistors, the amount of power transferred from the gyrotron cavity to the water cooling circuit could be calculated. For a gyrotron output power of 12.5 W at 460.38 GHz and a flow rate of 0.7 gpm, the ohmic loss was estimated to be 48 W, yielding an extraction efficiency of 21%. The beam parameters during this measurement were V_b = 12.9 kV and I_b = 105 mA with the main magnetic field at B = 8.423 T. Simulations using the thermal solver ePhysics [35] indicates that the cavity temperature would be about 10°C higher than the water temperature if one considers 48 W as the cavity thermal load, and perfect heat transfer between the water and the cooling channel copper wall. In this scenario, the gyrotron frequency would be downshifted by 78 MHz.

D. CW Long-Term Stable Operation

Continuous gyrotron operation for extended periods with stable power and frequency characteristics is an important requirement to allow long-term signal averaging in DNP/NMR experiments. The long-term stability of the 460 GHz gyrotron operating in the $TE_{11,2,1}$ mode was evaluated for a period of two days and the monitored variables are shown in Fig. 9. A quasi-optical directional coupler [36] was utilized at the end of the output corrugated waveguide to divert part of the output power to the frequency measurement system. The gyrotron output power was kept stable within ±0.7% by a computerized proportional, integral, and derivative (PID) control system implemented in LabVIEW that adjusted the cathode filament current based on the difference between a set point value and the output power monitored by a calibrated diode. This level of power fluctuation and the observed frequency stability of ±2.9 MHz (±6 ppm) are suitable for DNP/NMR. During the stability test, the main superconducting magnet was in persistent mode at B = 8.422 T, which has a magnetic field drift rate of less than 0.02 ppm/h according to a NMR probe measurement.

E. Output Beam Pattern

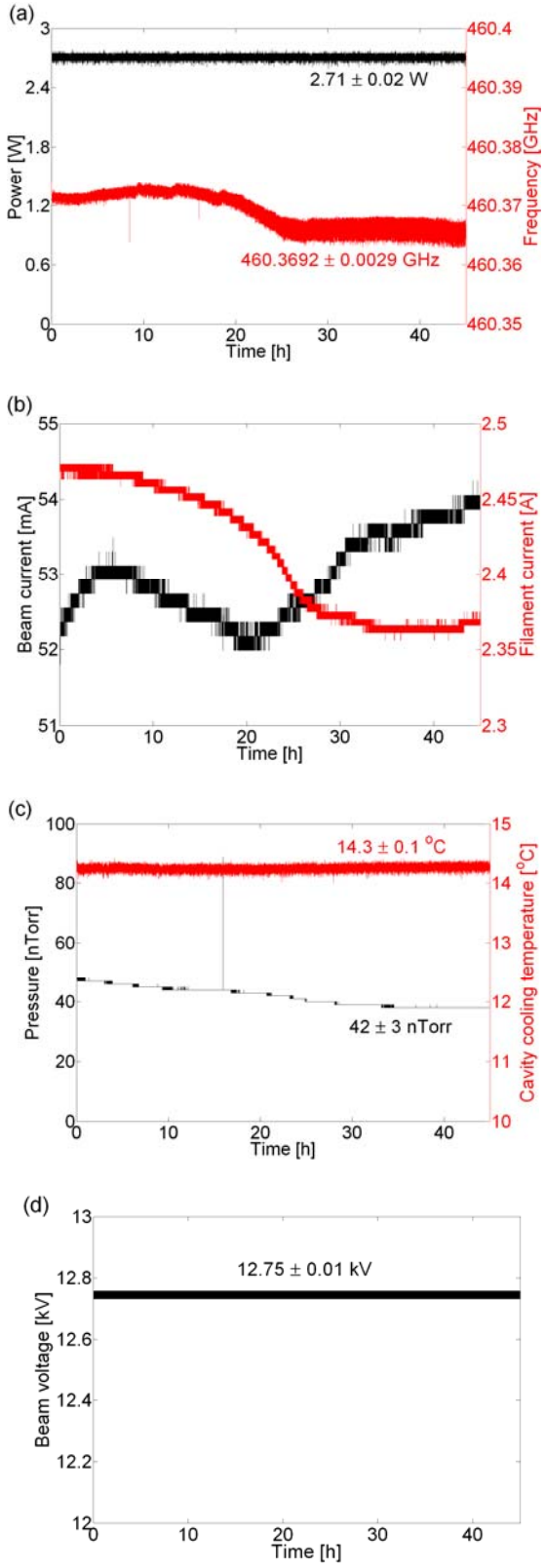

Fig. 9. Monitored variables during the long-term stability test of the 460 GHz gyrotron operating in the second-harmonic $TE_{11,2,1}$ mode: (a) output power and frequency, (b) beam and filament currents, (c) pressure and cavity cooling temperature, and (d) beam voltage. The main magnetic field was persistent at B = 8.422 T.

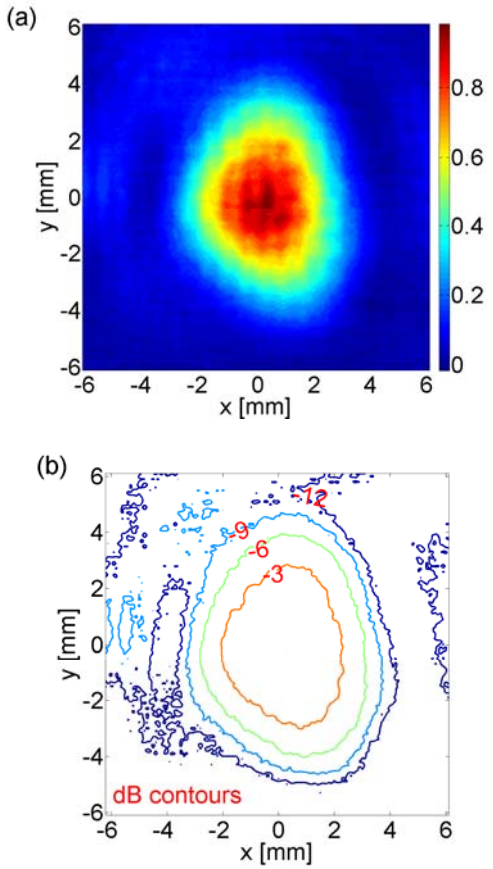

Fig. 10. Gyrotron output microwave beam displayed in (a) normalized linear power scale, and (b) dB contours. The pyroelectric camera image of the mode-converted $TE_{11,2}$ mode at 460.3 GHz was taken 40 mm after the end of the corrugated waveguide.

The gyrotron output beam pattern was measured by a Spiricon Pyrocam III pyroelectric camera positioned after the corrugated waveguide connected to the gyrotron window. The camera consists of an array of 124-by-124 $LiTaO_3$ pyroelectric sensors with a spacing of 100 μm between each pixel, yielding an active area of 12.4 by 12.4 mm. Since the pyroelectric sensors are only sensitive to alternating signals, the CW microwave beam was modulated at a rate of 24 or 48 Hz by a built-in chopper located over the detection area. During the camera measurements, the gyrotron output power was limited to 0.4 W, below the camera sensor damage threshold of 2 W.

An image of the $TE_{11,2}$ mode-converted beam at 460.3 GHz captured 40 mm after the end of the corrugated waveguide is displayed in Fig. 10. Based on the measured pattern, the Gaussian-like content associated with the measured microwave beam was computed to be 92% with beam radii w_x = 4.1 mm and w_y = 4.6 mm, corresponding to an ellipticity of 12%. Due to the limited access provided by the horizontal cross bore of the superconducting magnet, a direct beam measurement after the gyrotron window was not possible using the pyroelectric camera. However measurements performed with thermal paper inside the cross bore corroborated the camera results and confirmed the alignment of the output beam trajectory with respect to the cross bore centerline. These results indicate a good performance of the implemented internal quasi-optical converter from a whispering-gallery mode $TE_{11,2}$ to a Gaussian-like microwave beam at a submillimeter wavelength.

IV. Conclusion

The improved version of the 460 GHz second-harmonic gyrotron has generated 16 W of output power for a 13-kV 100-mA electron beam, yielding an efficiency of 1.2%. The minimum starting current of the operating mode $TE_{11,2,1}$ was measured to be 27 mA, agreeing with the linear theory prediction. Smooth frequency tunability of 1 GHz has been demonstrated for the operating second-harmonic mode as a function of the cyclotron frequency either by magnetic field tuning or beam voltage tuning. This frequency tuning range is twenty times broader than previously observed for a second-harmonic mode in a millimeter and submillimeter-wave gyrotron. A frequency tunable microwave source is highly desirable since it simplifies the implementation of DNP in NMR spectrometers, especially the ones without sweep coils. The stability characteristics of the gyrotron were evaluated during a period of 2 days in which the gyrotron operated continuously under computerized PID control monitoring the CW output power. Power stability of ±0.7% and frequency stability of ±2.9 MHz (±6 ppm) were obtained, which are suitable for the 700 MHz DNP/NMR application for which the gyrotron was designed. The Gaussian-like content of the mode-converted $TE_{11,2}$ output beam was calculated to be 92% with an ellipticity of 12%, indicating proper operation of the implemented internal quasi-optical mode converter.

References

[1] T. Maly, G. T. Debelouchina, V. S. Bajaj, K-N. Hu, C.-G. Joo, M. L. Mak-Jurkauskas, J. R. Sirigiri, P. C. A. van der Wel, J. Herzfeld, R. J. Temkin, and R. G. Griffin, "Dynamic nuclear polarization at high magnetic fields," *J. Chem. Phys.*, vol. 128, 052211, 2008.

[2] C.-G Joo, K.-N. Hu, J. A. Bryant, and R. G. Griffin, "In situ temperature jump high-frequency dynamic nuclear polarization experiments: enhanced sensitivity in liquid-state NMR spectroscopy," *J. Am. Chem. Soc.*, vol. 128, pp. 9428-9432, 2006.

[3] V. S. Bajaj, M. K. Hornstein, K. E. Kreischer, J. R. Sirigiri, P. P. Woskov, M. L. Mak-Jurkauskas, J. Herzfeld, R. J. Temkin, and R. G. Griffin, "250 GHz CW gyrotron oscillator for dynamic nuclear polarization in biological solid state NMR," *J. Magn. Reson.*, vol. 189, pp. 251-279, 2007.

[4] R. J. Trew, "High-frequency solid-state electronic devices," *IEEE Trans. Electron Devices*, vol. 52, pp. 638-649, May 2005.

[5] J. L. Hesler, D. S. Kurtz, Y. Duan, and T. W. Crowe, "Solid state sources, receivers and systems for plasma diagnostics and THz frequency extenders for VNAs," in *Proc. IEEE 36th Int. Conf. on Plasma Science*, San Diego, CA, Jun. 2009.

[6] A. K. Hassan, L. A. Pardi, J. Krzystek, A. Sienkiewicz, P. Goy, M. Rohrer, and L.-C. Brunel, "Ultrawide band multifrequency high-field EMR technique: a methodology for increasing spectroscopic information," *J. Magn. Reson.*, vol. 142, pp. 300-312, 2000.

[7] G. Dodel, "On the history of far-infrared (FIR) gas lasers: thirty-five years of research and application," *Infrared Phys. Technol.*, vol. 40, pp. 127-139, 1999.

[8] THz laser system, Coherent, Inc. Available: http://www.coherent.com/downloads/SIFIR50_DSrevB.pdf

[9] Infrared gas lasers, Edinburgh Instruments. Available: http://www.edinst.com/pdf/infraredgaslaser.pdf

[10] Extended-interaction oscillators, Communications and Power Industries Inc. Available: http://www.cpii.com/docs/library/7/general.pdf

[11] G. Kantorowicz, and P. Palluel, "Backward wave oscillators," in *Infrared and Millimeter Waves*, vol. 1, K. J. Button, Ed. New York: Academic Press, 1979, pp. 185-212.

[12] A. Kasugai, K. Sakamoto, K. Takahashi, K. Kajiwara, and N. Kobayashi, "Steady-state operation of 170 GHz–1 MW gyrotron for ITER," *Nucl. Fusion*, vol. 48, 054009, 2008.

[13] M. Thumm, "State-of-the art of high power gyro-devices and free electron masers, Update 2007," Scientific Report FZKA 7392, Forschungszentrum Karlsruhe, Germany, Mar. 2008.

[14] N. I. Zaytsev, T. B. Pankratova, M. I. Petelin, and V. A. Flyagin, "Millimeter- and submillimeter-wave gyrotrons," *Radio Eng. Electron. Phys.*, vol. 19, pp. 103-107, May 1974.

[15] L. R. Becerra, G. J. Gerfen, R. J. Temkin, D. J. Singel, and R. G. Griffin, "Dynamic nuclear polarization with a cyclotron resonance maser at 5 T," *Phys. Rev. Lett.*, vol. 71, no. 21, pp. 3561-3564, Nov. 1993.

[16] K. Kreischer, C. Farrar, R. Griffin, R. Temkin, and J. Vieregg, "250 GHz gyrotron for NMR spectroscopy," in *Proc. IEEE 27th Int. Conf. on Plasma Science*, New Orleans, LA, Jun. 2000, p. 198.

[17] C. D. Joye, R. G. Griffin, M. K. Hornstein, K.-N. Hu, K. E. Kreischer, M. Rosay, M. A. Shapiro, J. R. Sirigiri, R. J. Temkin, and P. P. Woskov, "Operational characteristics of a 14-W 140-GHz gyrotron for dynamic nuclear polarization," *IEEE Trans. Plasma Sci.*, vol. 34, no. 3, pp. 518-523, Jun. 2006.

[18] T. Idehara, I. Ogawa, L. Agusu, T. Kanemaki, S. Mitsudo, T. Saito, T. Fujiwara, and H. Takahashi, "Development of 394.6 GHz CW gyrotron (gyrotron FU CW II) for DNP/proton-NMR at 600 MHz," *Int. J. Infrared Millim. Waves*, vol. 28, pp. 433-442, 2007.

[19] M. Silva, S. Alberti, J.-P. Ansermet, K. A. Avramides, G. Bodenhausen, J.-P. Hogge, I. Pagonakis, and D. Wagner, "Design of a low-power high-frequency gyrotron for DNP-enhanced NMR spectroscopy," in *Proc. IEEE 35th Int. Conf. on Plasma Science*, Karlsruhe, Germany, Jun. 2008, p. 4590845.

[20] T. Idehara, L. Agusu, I. Ogawa, S. Kobayashi, T. Saito, R. Dupree, and M. E. Smith, "Development of gyrotron FU CW IIA for 600 MHz and 300 MHz DNP-NMR experiments at the University of Warwick," in *Proc. 33rd Int. Conf. on Infrared, Millimeter and Terahertz Waves*, Pasadena, CA, Sept. 2008, p. 46654233.

[21] 263 GHz solid state DNP-NMR spectrometer, Bruker Biospin. Available: http://www.bruker-biospin.com/dnp-dir.html

[22] M. K. Hornstein, V. S. Bajaj, R. G. Griffin, K. E. Kreischer, I. Mastovsky, M. A. Shapiro, J. R. Sirigiri, and R. J. Temkin, "Second harmonic operation at 460 GHz and broadband continuous frequency tuning of a gyrotron oscillator," *IEEE Trans. Electron Devices*, vol. 52, no. 5, pp. 798-807, May 2005.
[23] M. K. Hornstein, V. S. Bajaj, R. G. Griffin, and R. J. Temkin, "Continuous-wave operation of a 460-GHz second harmonic gyrotron oscillator," *IEEE Trans. Plasma Sci.*, vol. 34, no. 3, pp. 524-533, Jun. 2006.
[24] T. Idehara, I. Ogawa, H. Mori, S. Kobayashi, S. Mitsudo, and T. Saito, "A THz gyrotron FU CW III with a 20 T superconducting magnet," in *Proc. 33rd Int. Conf. on Infrared, Millimeter and Terahertz Waves*, Pasadena, CA, Sept. 2008, p. 4665652.
[25] T. H. Chang, T. Idehara, I. Ogawa, L. Agusu, and S. Kobayashi, "Frequency tunable gyrotron using backward-wave components," *J. Appl. Phys.*, vol. 105, 063304, 2009.
[26] S. V. Samsonov, G. G. Denisov, V. L. Bratman, A. A. Bogdashov, M. Y. Glyavin, A. G. Luchinin, V. K. Lygin, and M. K. Thumm, "Frequency-tunable CW gyro-BWO with a helically rippled operating waveguide," *IEEE Trans. Plasma Sci.*, vol. 32, no. 3, pp. 884-889, Jun. 2004.
[27] W. B. Hermannsfeldt, "EGUN - an electron optics and gun design program," Technical report SLAC-331 UC-28, Stanford Linear Accelerator Center, Oct. 1988.
[28] A. W. Fliflet, and M. E. Read, "Use of weakly irregular waveguide theory to calculate eigenfrequencies, Q values, and RF field functions for gyrotron oscillators," *Int. J. Electron.*, vol. 51, no. 4, pp. 475-484, 1981.
[29] M. Blank, B. G. Danly, B. Levush, P. E. Latham, and D. E. Pershing, "Experimental demonstration of a W-band gyroklystron amplifier," *Phys. Rev. Lett.*, vol. 79, no. 22, pp. 4485-4488, Dec. 1997.
[30] M. Yedulla, G. S. Nusinovich, and T. M. Antonsen, Jr., "Start currents in an overmoded gyrotron," *Phys. Plasmas*, vol. 10, no. 11, pp. 4513-4520, Nov. 2003.
[31] Cascade engine v1.60, Calabazas Creek Research, Inc., Saratoga, CA, 2001.
[32] S. N. Vlasov, L. I. Zagryadskaya, and M. I. Petelin, "Transformation of a whispering gallery mode propagating in a circular waveguide into a beam of waves," *Radio Eng. Electron. Phys.*, vol. 20, pp. 14-17, 1975.
[33] J. M. Neilson, and R. Bunger, "Surface integral equation analysis of quasi-optical launcher," *IEEE Trans. Plasma Sci.*, vol. 30, no. 3, pp. 794-799, Jun. 2002.
[34] P. P. Woskov, M. K. Hornstein, R. J. Temkin, V. S. Bajaj, and R. G. Griffin, "Transmission lines for 250 and 460 GHz CW gyrotron DNP experiments," in *Proc. Joint 30th Int. Conf. on Infrared and Millimeter Waves*, Williamsburg, VA, Sept. 2005, pp. 563-564.
[35] ePhysics. Version 2.0, Ansoft Corporation, Pittsburg, PA, 2006.
[36] P. P. Woskov, V. S. Bajaj, M. K. Hornstein, R. J. Temkin, and R. G. Griffin, "Corrugated waveguide and directional coupler for CW 250-GHz gyrotron DNP experiments," *IEEE Trans. Microw. Theory Tech.*, vol. 53, no. 6, pp. 1863-1869, Jun. 2005.